
AN EFFECTIVE LOSS FUNCTION FOR GENERATING 3D MODELS FROM SINGLE 2D IMAGE WITHOUT RENDERING

MARCH 7, 2022

Nikola Zubić*

Faculty of Technical Sciences
Novi Sad, Serbia
nikola.zubic@uns.ac.rs

Pietro Liò

University of Cambridge
Cambridge, United Kingdom
pietro.liò@cst.cam.ac.uk

ABSTRACT

Differentiable rendering is a very successful technique that applies to a Single-View 3D Reconstruction. Current renderers use losses based on pixels between a rendered image of some 3D reconstructed object and ground-truth images from given matched viewpoints to optimise parameters of the 3D shape.

These models require a rendering step, along with visibility handling and evaluation of the shading model. The main goal of this paper is to demonstrate that we can avoid these steps and still get reconstruction results as other state-of-the-art models that are equal or even better than existing category-specific reconstruction methods. First, we use the same CNN architecture for the prediction of a point cloud shape and pose prediction like the one used by Insafutdinov & Dosovitskiy. Secondly, we propose the novel effective loss function that evaluates how well the projections of reconstructed 3D point clouds cover the ground truth object's silhouette. Then we use Poisson Surface Reconstruction to transform the reconstructed point cloud into a 3D mesh. Finally, we perform a GAN-based texture mapping on a particular 3D mesh and produce a textured 3D mesh from a single 2D image. We evaluate our method on different datasets (including ShapeNet, CUB-200-2011, and Pascal3D+) and achieve state-of-the-art results, outperforming all the other supervised and unsupervised methods and 3D representations, all in terms of performance, accuracy, and training time.

1 Introduction

One of the main problems in 3D Computer Graphics and Vision is the ability of a model to learn 3D structure representation and reconstruction [11, 24]. Supervised 3D Deep Learning is highly efficient in direct learning from 3D data representations [1], such as meshes, voxels, and point clouds. They require a large amount of 3D data for the training process, and also, their representation is sometimes complex for the task of direct learning. These factors lead to the abandonment of this approach because of its inefficient performance and time consumption. Unsupervised 3D structural learning [8] learns 3D structure without 3D supervision and represents a promising approach.

Differentiable rendering is a novel field that allows the gradients of 3D objects to be calculated and propagated through images [13]. It also reduces the requirement of 3D data collection and annotation, while enabling a higher success rate in various applications. Their ability to create a bond between 3D and 2D representations, by computing gradients of 2D loss functions with the respect to 3D structure, makes them a key component in unsupervised 3D structure learning. These loss functions are based on differences between RGB pixel values [15]. By rendering the predicted 3D structure from a specific viewpoint and then evaluating the loss function based on pixel-wise loss between rendered and ground truth image, model parameters are optimised to reconstruct the desired 3D structure. This structure needs, by definition of this problem, to be consistent with the ground truth image. For evaluation of this type of loss function, previous techniques used interpolation [3], rasterisation-based rendering [21] and visibility handling [22].

However, these evaluation techniques are very time-consuming. They don't contribute at all to an accurate 3D structure reconstruction. Here, we propose a novel idea for fast 3D structure reconstruction (in the form of a point cloud

*Work performed while the author was Research Intern Apprentice under the supervision of professor Pietro Liò.

silhouette) and then we convert it to a 3D mesh and transfer the object’s texture from a 2D image onto the reconstructed 3D object. Hence, unlike in loss functions that are based on pixels, our approach has an effective loss function that arises exclusively from the 2D projections of 3D points, without interpolation based on pixels, shading and visibility handling.

2 Why point clouds?

Because of their compactness, point clouds are considered as one of the three most popular 3D representations and are studied well in the field of 3D Deep Learning. Generation of the point cloud is less time-consuming and more efficient than voxelisation [4]. Point cloud models can accurately represent relatively complex objects with a finite number of elements (points). Our method can be used to generate point clouds that contain an arbitrary number of 3D points. We produce a loss for each point without rendering. One of the factors, why we use point clouds, is regarding the performance and fact that they can be automatically transformed to 3D meshes [14]. Then, on these meshes, a texture mapping will be applied.

3 Related work

3.1 3D representations

Previous works [29, 35] have concentrated on mesh reconstruction by using the full 3D supervision approach. The main problem with these approaches, besides inefficiency, is the usage of ground-truth 3D meshes, and they are mostly available in a limited number of datasets, fully computer-generated which can sometimes make output blurry if we input real-world images. Some approaches [30, 31] solved this problem by using 2D supervision from multiple-scene images based on voxels. Recent approaches call off the requirement of multiple views to learn single-view 3D reconstruction by using either voxel [4] or mesh [21] representation. However, point cloud representation is the most effective because of its computational efficiency and ability to retain the structure with a certain number of points that form a point cloud [10]. Their only problem is the rendering step. Our approach omits a rendering step.

3.2 Differentiable rendering

Prediction of 3D models from single images while achieving high-quality visual results is possible by using the differentiable renderer. A differentiable rendering framework allows gradients to be analytically (or approximately) computed for all pixels in an image. RenderNet [25] is a differentiable rendering convolutional network with a projection unit that can render 2D images from 3D shapes and automatically encodes spatial occlusion and calculates shading. These calculations are also time-consuming. OpenDR [22] is the pioneer of differentiable rasterisation-based renderers and approximates gradients with the respect to pixel positions by using the first-order Taylor approximation. Soft-Rasterizer [21] introduces a probabilistic formulation of the rasterisation process, where each pixel is assigned softly to all faces of the mesh. While inducing a higher computational cost, this trick analytically allows gradient computation. However, a complete differentiable rendering pipeline has serious time consumption and inefficiency problems.

3.3 Unsupervised learning of shape and pose with differentiable point clouds

The work that inspired us addresses the learning of an accurate 3D shape and camera pose from a collection of unlabeled category-specific images [10]. It uses a specific convolutional neural network architecture to predict both model’s shape and the pose from a single image. To deal with the pose ambiguity problem, it introduces an ensemble of pose predictors. This ensemble distills to a single "student" model. It uses the same representation we used as the initial one (point clouds) and allows differentiable projection. The experiments showed that the distilled ensemble of pose predictors learns to estimate the pose accurately, while the point cloud representation allows predicting detailed shape models. However, it is still time-consuming since it uses differentiable point cloud projection.

4 Proposed method

4.1 Intuitive overview

Deep learning based on the 3D structure has made significant progress. Now, it is possible to learn more about explicit 3D representations and create a bridge between 2D and 3D space. Recently, some methods have introduced the

possibility of learning 3D shapes as implicit functions, such as using a deep learning model to "learn" the mapping of signed distances [20] based on 3D locations.

In order to overcome the problems of structural 3D learning, unsupervised methods introduced different differentiable renderers [10, 11, 13, 3, 21, 22, 25] to first render the reconstructed 3D shape into 2D images from different view-angles and then portray them as what got obtained through complete supervision. After this, we can calculate the pixel-wise losses between those 2D images from different view-angles and real (ground-truth) images from the dataset. Since the renderer is differentiable, the loss between these images back-propagates through the network to train it.

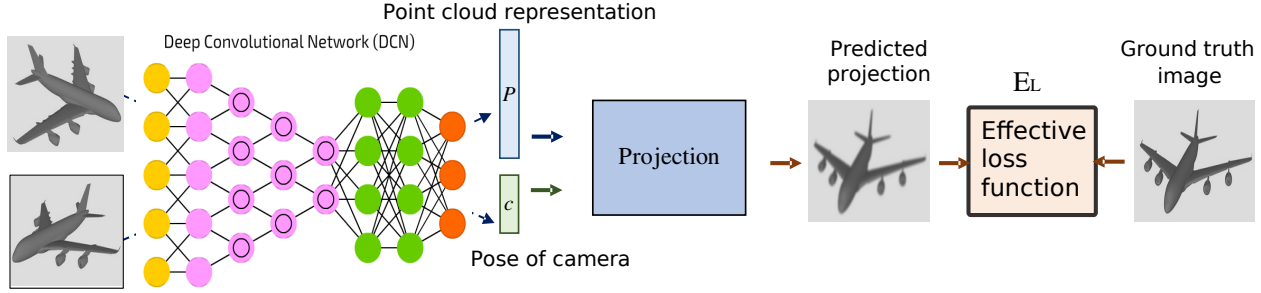


Figure 1: Our method removes the rendering process and requires only 2D projections of 3D point clouds. During the generation of 3D shapes using multiple silhouette images (from different viewing angles), 2D projections of all points on the shape should uniformly cover the silhouette from each viewing angle. We implement this using two key ideas (that together form effective loss function). (1) For 3D shapes formed by 3D points, their projections for each view should locate within the silhouette. (2) All projections for each silhouette should distribute uniformly. We achieve this by maximising the loss between each of the pairs of these 2D projections. \mathbf{P} - Point cloud representation, \mathbf{c} - Pose of camera.

To evaluate the pixel-wise loss, previous differentiable renderers rendered the images by taking into account some form of interpolation [3] of the reconstructed 3D structure over each pixel, such as rasterisation and visibility handling.

We train a network that learns to generate a 3D point cloud based on a single image using the images from a dataset (from different view-angles) as supervision which is opposed to those that use ground-truth point clouds as supervision. Current methods render based on differentiable renderers that render images of the reconstructed 3D shape and actual images and then minimise the pixel-wise loss to optimise the reconstructed 3D shape.

Total effective loss informs us how well the projected points cover the objective silhouette. The process includes two terms, one that forces all the projections into the silhouette where the projections initialise randomly, and the other term forces each pair of projections from each other as much as possible, which allows the projections to cover the silhouette uniformly. Starting from some point cloud (randomly initialised), we can force all the projections in the silhouette using the first term, and then using the second term, we can uniformly distribute projections to cover the whole silhouette.

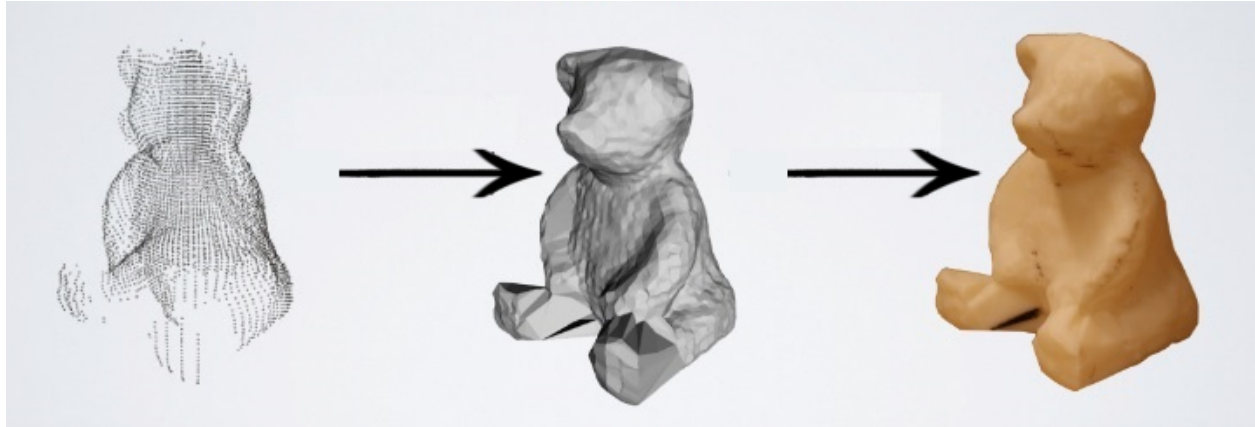


Figure 2: Generated 3D point cloud is transformed into 3D mesh and then textured.

After completing the process shown in Figure 1, we generate 3D point cloud for a desired image. After this, we apply Poisson Surface Reconstruction [14] to generate 3D mesh from given 3D point cloud and then we use GAN for texture mapping on a particular 3D mesh and produce a textured 3D mesh based on the input image texture, which is shown in the Figure 2.

4.2 Implementation details

Camera parameters describe the mathematical relationship between 3D coordinates of a point located within a scene and the 2D coordinates of its projection on the plane of the image (because of present light emission). Internal (intrinsic) parameters relate to the camera itself (focal length, lens distortion). External (extrinsic) parameters describe the transformation between the camera and the outside world (camera pose). In this approach, we represent 3D point clouds in an object-centered coordinate system [19]. Using the perspective’s transformation, we begin by transforming the coordinates of every point. Results are available in .obj format in Blender [6].

Our goal is to learn the structure of 3D point clouds (P) formed by N points n_j only from G_t ground-truth images of the silhouette S_i , where $j \in [1, N]$ and $i \in [1, G_t]$. Current differentiable renderers rely on point clouds (P) rendering into raster images S'_i from i -th viewing angle, which are used to produce a loss by comparing S'_i i S_i pixel by pixel. These steps are not necessary to get a precise solution.

Let the projection of the point n_j in view i be p_j^i . The error evaluates how well the sets of projected points $\{p_j^i \mid j \in [1, N]\}$ cover the silhouette of the object. So, the loss is composed of two parts.

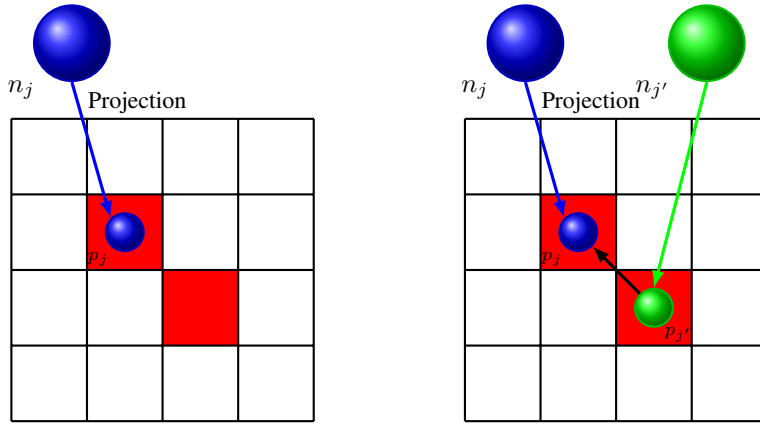


Figure 3: The left and right grids represent two ground-truth silhouette images S_i . n_j point projects onto an image, and its projection is p_j . **Left:** For 3D shapes formed by 3D points, their projections for each view should locate within the silhouette, where the whole white grid is a silhouette, and its pixel values are 1 (red square). So, we are minimising differences between pixel values of projections and 1 for every projection. **Right:** Besides that, we must not only minimise the first term loss but also the second term loss which maximises the distance between different projections p_j and $p_{j'}$.

If we have a predicted 3D point cloud and a binary image of the silhouette, the loss calculates as follows: First, we project the points p_j (we write abbreviated, this is p_j^i) on the images of the silhouette S_i , where the pixel value of the projection p_j is denoted by π_i . The first term penalises points outside of the foreground by calculating the difference $1 - \pi_i(p_j)$, assuming that the foreground in the binary silhouette image has a value of 1. Minimising this loss will force all projections into the foreground. Additionally, the second term adjusts the spatial distribution of the projected points. It forces the pairs of projections in the foreground to be as far apart from each other as possible (right grid shown in the Figure 3). Thus, such a system arranges the 3D locations of the points n_j through their projections p_j by simultaneously optimising these two losses.

The first term is calculated as the difference between 1 and the value $\pi_i(p_j^i)$ of each projection p_j^i on the silhouette image S_i . We make use of bilinear interpolation to calculate the value $\pi_i(p_j^i)$ using the binary pixel values of the nearest pixels around p_j^i . All projections are forced to the foreground for all silhouette images by minimising the following loss:

$$L_1(p_j^i, \pi_i) = \|1 - \pi_i(p_j^i)\| \quad (1)$$

However, it is impossible to force all projections into the foreground by minimising this $L1$ loss. If we optimise point cloud according to some silhouette image (a) and start from some randomly initialised points (b), then we will get inadequate point projections if we use $L1$ loss, as shown in the Figure 4.

There are two reasons why this problem occurs. One reason is the fact that $L1$ loss is non-differentiable. Even if we only look at the difference, the second reason is that we only examine the pixel intensity based on the difference between 1 and the interpolated pixel value $\pi_i(p_j^i)$ based on the four closest binary pixel values. This prevents training if the projections p_j^i are too far from the foreground.

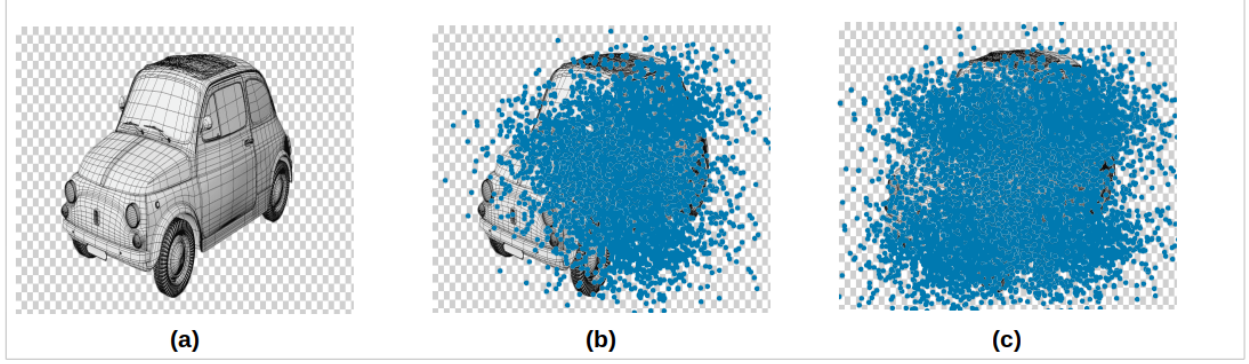


Figure 4: We are given a silhouette image (a) and randomly initialized projections (b). Then we cannot force projections into the foreground (c) because standard first term loss has a local minimum problem, which results in a non-uniform disposition of projections (blue dots). This problem is solved by smoothing the original silhouette to obtain pixel values of projections and calculate the difference.

Our goal is to produce non-zero gradients anywhere in the background part, while the pixel values in the foreground part do not require a modification. For each pixel x_{RGB} on the background π_i^G , we write:

$$\pi_i^G(x_{RGB}) = \begin{cases} 1, & x_{RGB} \in \mathcal{B} \\ 1 - d(x_{RGB}, \partial\mathcal{B}), & x_{RGB} \in \bar{\mathcal{B}} \end{cases} \quad (2)$$

where $\mathcal{B} = \{x_{RGB} \mid \pi_i(x_{RGB}) = 1\}$ is the foreground, while $\bar{\mathcal{B}} = \{x_{RGB} \mid \pi_i(x_{RGB}) = 0\}$ is a background, and $\partial\mathcal{B}$ is the foreground's boundary. $d(x_{RGB}, \partial\mathcal{B})$ represents the L_2 distance between x_{RGB} and his closest $\partial\mathcal{B}$, which is normalised by the resolution π_i .

We will denote these processed silhouette images as π_i^G , to distinguish between the original silhouette image S_i and the processed image. Normalisation is also performed on the processed pixel values in the background for them to lie in the interval $(0, 1)$. Min-max normalisation is used for this sub-task: $\pi_i^G(\bar{\mathcal{B}}) = \min_{\max}(v_i^G(\bar{\mathcal{B}}))$. Finally, the modified first term loss function is:

$$\mathcal{M}_1(p_j^i, \pi_i) = \|1 - \pi_i^G(p_j^i)\| \quad (3)$$

According to Figure 5, using only the first term loss leads to non-uniform point projections in the foreground. To accurately represent the 3D shape and cover the silhouette, we will use a second term loss. Through this loss, we will model the spatial relationship between every two pairs of projections. That loss should force projections inside the foreground. They should be as far away from each other as possible.

However, the second term loss is, to some extent, in conflict with the first term loss, which tries to force all projections close, especially near the foreground boundaries. Near the foreground boundaries, it is harder to force two projections apart than inside the foreground without forcing them into the background. To solve this problem, we propose a second-term loss function that increases the distance between projection pairs that are deeper within the foreground and reduces it for projection pairs around the foreground boundary. It skips projections within the background.

For every projection pair p_j^i and $p_{j'}^i$, the $L2$ distance is calculated by the formula:

$$d(p_j^i, p_{j'}^i) = \|p_j^i - p_{j'}^i\|_2, \quad (4)$$

which we then normalise according to the resolution of the silhouette image. This approach tends to maximise the distance $d(p_j^i, p_{j'}^i)$. We use the Gaussian function [17] to obtain a loss based on the invariance of the structure which

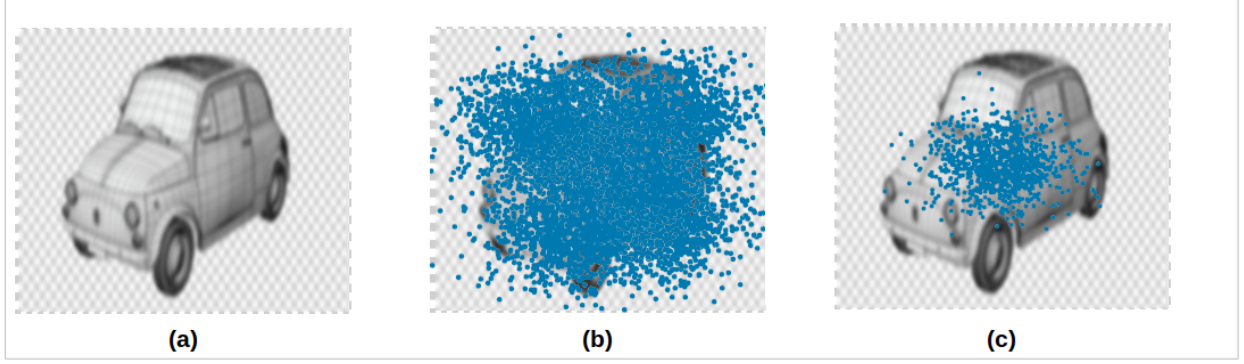


Figure 5: With modified first term loss function, it is possible to force all projections of randomly initialised points **(b)** from a smoothed silhouette image **(a)** into the foreground **(c)** by minimising the equation 3. Blue dots represent the projections.

decreases with increasing the distance. So, we can essentially minimise the loss of invariance along with the modified first term loss \mathcal{M}_1 .

For each projection p_j^i , loss based on the invariance of the structure models its spatial relationship with all other projections $p_{j'}^i$:

$$\mathcal{L}_2(p_j^i, \{p_{j'}^i\}, \pi_i) = w_j^i \sum_{j'=1}^N \left[w_{j'}^i \cdot \exp\left(\frac{-d(p_j^i, p_{j'}^i)}{\theta} + \mu_j^i\right) \right], \quad (5)$$

where w_j^i and $w_{j'}^i$ are weights corresponding to the projections p_j^i and $p_{j'}^i$, respectively, θ is the decay parameter, μ_j^i is the boundary bias for the projection p_j^i .

w_j^i expresses to what level the projection p_j^i merges with the background. If that weight is set to zero, the projection p_j^i is such that the invariance of the structure is completely removed so that the modified first term loss \mathcal{M}_1 immediately forces p_j^i within the foreground. The decay (merge) parameter controls the merge interval (invariance of the structure intensity) of a given background 3D model. The projection boundary bias μ_j^i for projection p_j^i controls the distance to the foreground's boundary where the invariance over that projection reduces.

Weight w_j^i is calculated using bilinear interpolation based on the closest binary pixel values in the silhouette image S_i , as shown in the Figure 3. We use multi-scale gradients [27] to compute μ_j^i . Binary pixel values are extracted from adjacent points located at the vertices of the squares in the grid (around the projection p_j^i) - Figure 3. We perform interpolations over them, and we take the mean value of all of these interpolations to calculate μ_j^i . This approach progressively reduces invariance of the structure as p_j^i approaches the foreground's boundary.

Finally, the effective loss function E_L is calculated through simultaneous minimisation of the modified first term loss function \mathcal{M}_1 and the second term loss function \mathcal{L}_2 based on the invariance of the structure. The total error E_L is obtained by the following formula (α and β are used for balancing the losses, average over points and views):

$$E_L = \frac{\sum_{i=1}^{G_t} \sum_{j=1}^N (\alpha \mathcal{M}_1(p_j^i, \pi_i) + \beta \mathcal{L}_2(p_j^i, \{p_{j'}^i\}, \pi_i))}{G_t \cdot N} \quad (6)$$

The main goal of the effective loss function is to demonstrate how well projected points cover a foreground (object's silhouette). This function is composed of two parts in which one part is forcing the projection of every 3D point on the foreground, while the other part forces every projection pair which lies inside a foreground to be as far away as possible, as shown in the Figure 3. This enables the whole foreground to be covered and prohibits points from needlessly accumulating near each other.

After this process, we have a 3D point cloud which is then transformed to a 3D mesh using Poisson Surface Reconstruction [14]. We use GAN [36, 16] for texture mapping on a particular 3D mesh and produce a textured 3D mesh based on the input image texture, which is shown in Figure 2. The generator generates displacement maps and textures, and the discriminator discriminates between real/fake displacement maps and textures.

5 Datasets, metrics & code

Datasets We used the following datasets: ShapeNet [2] (train/test split from [10]), CUB-200-2011 [32] (train/test split from [12]), and Pascal3D+ dataset [37] (train/test split from [12]).

Metrics Numerical evaluation is performed by using Chamfer’s distance [28] between predicted and real (ground-truth) point clouds:

$$d_{Chamfer}(P_1, P_2) = \frac{1}{|P_1|} \sum_{r \in P_1} \min_{s \in P_2} \|r - s\|_2 + \frac{1}{|P_2|} \sum_{s \in P_2} \min_{r \in P_1} \|s - r\|_2, \quad (7)$$

where P_1 is the predicted point cloud and P_2 is the ground-truth point cloud, r is a point on P_1 and s is a point on P_2 . $|P_1|$ and $|P_2|$ represent the number of points for point clouds P_1 and P_2 . The first sum evaluates the precision of the predicted point cloud by computing how far on average is the closest ground truth point from a predicted point. The second sum measures the coverage of the ground truth by the predicted point cloud: how far is on average the closest predicted point from a ground truth point [10].

When comparing with voxel-based results, we discretise the 3D space, where the predicted or the ground-truth point clouds are located, into a 3D voxel grid, where a voxel is set to 1 if it contains a point. Volumetric IoU [26] comparison is used by comparing the 3D grid voxelised from the predicted point cloud with the one voxelised from the ground truth point cloud.

Fréchet Inception Distance (FID) is widely used as an evaluation metric [9] (not only for 2D GANs but also for our task [39]). FID scores will evaluate 2D projections of generated point clouds to meshes. 3D mesh and textures are evaluated separately in this process.

Code Code, data and trained models will be available at: <https://github.com/NikolaZubic/2dimageto3dmodel>

6 Results and discussion

The quantitative results using Chamfer’s distance [28] are shown in Table 1. Our point cloud output (Ours) outperforms its voxel equivalent (Ours-V) in all cases. Chamfer’s distance improves with the increase of resolution. We also outperform the previous best method that used rendering [10] and DRC method [30].

	DRC [31]	Resolution 32			Resolution 64		Resolution 128	
		DPC [10]	Ours-V	Ours	DPC [10]	Ours	DPC [10]	Ours
Airplane	8.35	4.52	4.49	3.99	3.50	3.15	2.84	2.63
Car	4.35	4.22	3.75	3.79	2.98	2.86	2.42	2.37
Chair	8.01	5.10	5.34	4.64	4.15	3.99	3.62	3.46
Mean	6.90	4.61	4.53	4.14	3.55	3.33	2.96	2.82

Table 1: Quantitative results on shape prediction with known camera pose (on ShapeNet dataset). We report the Chamfer’s distance between normalised point clouds, multiplied by 100 and use three categories: Airplanes, Cars and Chairs. Our point cloud output outperforms all other methods in terms of Chamfer’s distance. Lower value is better; bold = best.

Our results outperform state-of-the-art differentiable renderers in the Volumetric IoU metric [26] while simultaneously being less time-consuming during the training phase, as shown in Table 2. For cars, our outcome is better than renderers based on voxels but very similar to renderers based on meshes because meshes represent a superior initial 3D representation for large areas of flat surfaces [12] (such as cars).

	Unsupervised learning			Supervised learning							
	SoftRas [21]	DIB-R [3]	Ours	P2M [33]	IN [18]	RN [5]	AN [7]	DSN [38]	3DN [34]	ON [23]	Ours
Airplane	58.4	57.0	62.4	51.5	55.4	42.6	39.2	57.5	54.3	57.1	75.3
Car	77.1	78.8	75.6	50.1	74.5	66.1	22.0	74.3	59.4	73.7	75.1
Chair	49.7	52.7	58.3	40.2	52.2	43.9	25.7	54.3	34.4	50.1	57.8
Mean	61.7	62.8	65.43	47.3	60.7	50.9	29.0	62.0	49.4	60.3	64.97

Table 2: Quantitative Volumetric IoU [26] comparison with differentiable renderers for different 3D representations and supervised methods (on ShapeNet dataset). We use three categories: Airplanes, Cars and Chairs. Bigger value is better; bold = best.

Table 3: Training time efficiency in hours.

	3D representations	Rendering	32 ² image 2000 points/ 32 ³ voxels	64 ² image 8000 points/ 64 ³ voxels	128 ² image 16000 points/ 128 ³ voxels
DRC [31]	Voxels	Yes	≈14h	≈60h	≈216h
DPC [10]	Point clouds	Yes	≈14h	≈24h	≈72h
Ours	Point clouds	No	≈ 6.5h	≈ 11h	≈ 34.5h

Table 4: FID scores on Mesh (produced from 3D point cloud), Texture (extracted by a GAN) and Both (final output - textured 3D mesh) grouped by dataset, texture resolution, and condition, both in truncated and untruncated cases. Lower is better; bold = best in that dataset.

Dataset	Texture resolution	Condition	σ	FID (truncated σ)			FID (untruncated)		
				Both	Tex.	Mesh	Both	Tex.	Mesh
CUB-200-2011	512x512	None	1	40.33	43.73	17.89	52.12	46.72	25.74
		Class	0.25	33.61	26.67	18.53	40.49	29.97	22.25
	256x256	Class	0.25	32.28	29.62	18.88	41.11	32.01	23.41
Pascal3D+	512x512	None	1	40.99	30.76	27.17	60.08	45.55	41.33
		Class	0.75	26.23	21.89	22.96	48.98	29.98	34.11
		Class + Colour	0.5	30.50	21.10	26.86	51.65	30.20	36.30
	256x256	Class + Colour	0.5	38.19	25.43	35.71	63.06	36.02	46.29

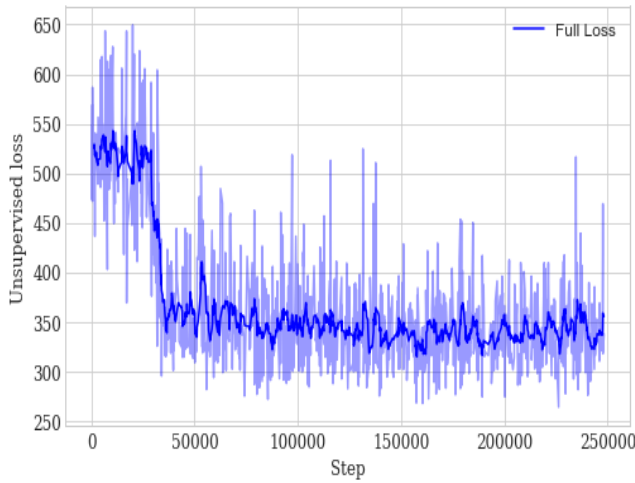


Figure 6: Total unsupervised loss decreases through time (more steps of training) which is an indicator that our model is learning the desired objective if we assume that objective is correctly set up.

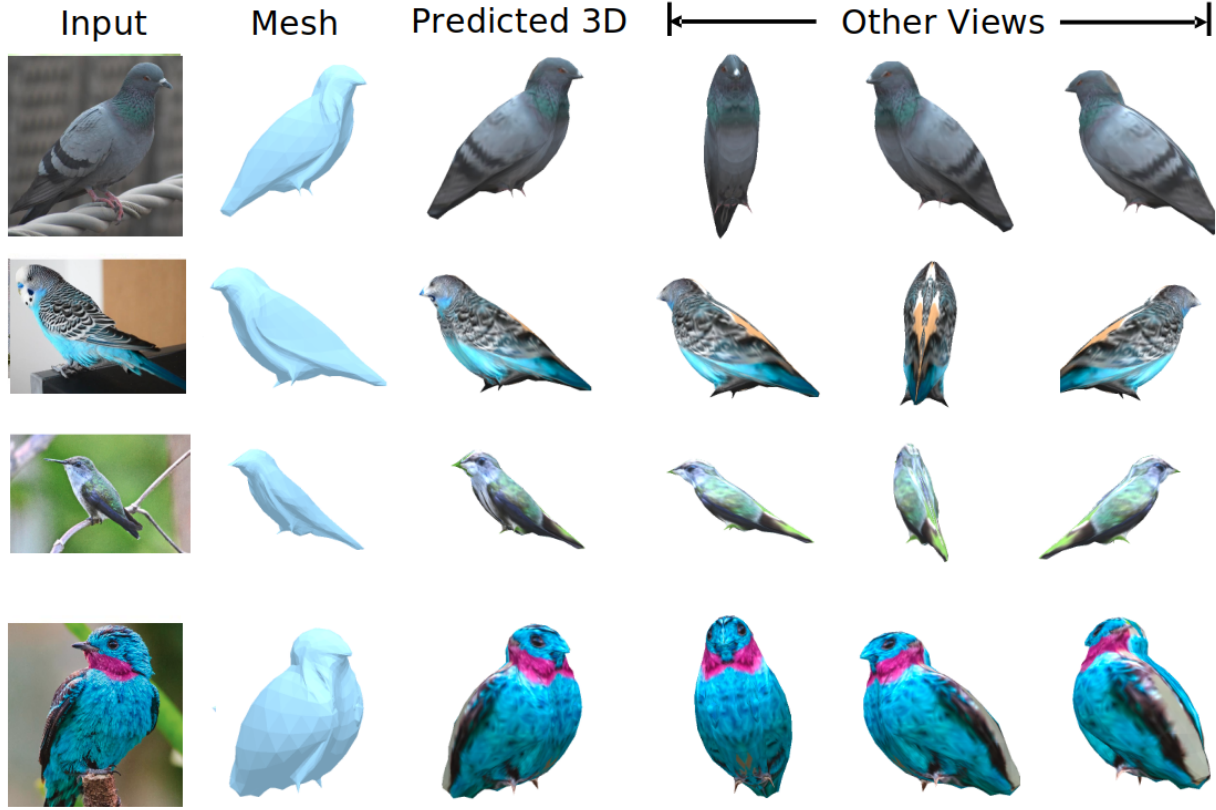


Figure 7: We use real-world 2D bird images as input for generating a 3D model. In the first column is the input where we have images of the real birds, in the second column, there is a generated 3D mesh (obtained from 3D point cloud after Poisson Surface Reconstruction [14]), and in the next four columns, there is a predicted 3D model visible in 4 poses.

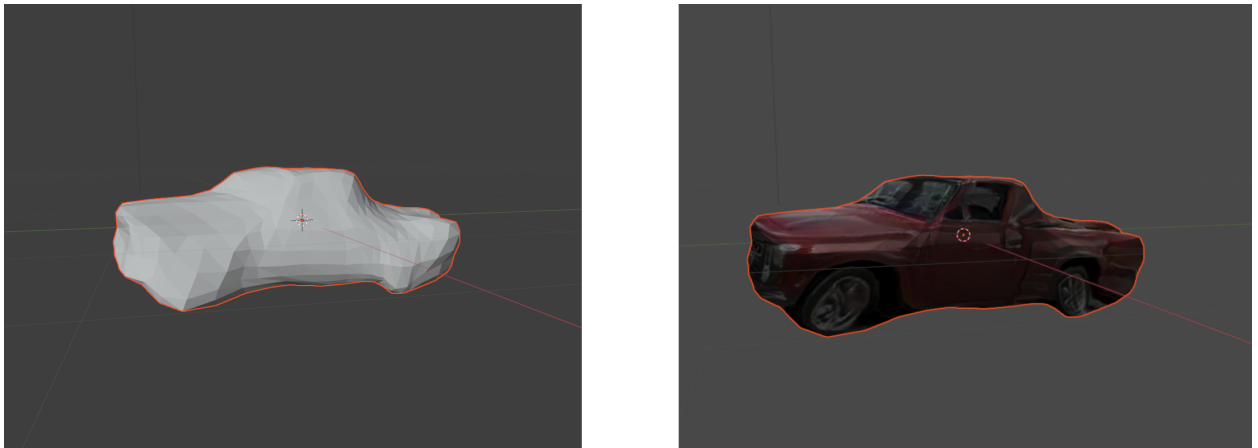


Figure 8: All generated 3D models can be visualised in the Blender tool [6] and viewed in real-time from an user-free angle. **Left:** 3D mesh without texture. **Right:** Textured 3D mesh which represents the final output of our model based on a single (in this case: car) image.

7 Conclusion

In this paper, we proposed a 3D reconstruction based on a single image, a method for learning the pose and shape of 3D objects given only their 2D projections, using the initial point cloud representation and then converting that representation to a 3D mesh. Mesh is textured using GANs to produce the final output. Extensive experiments have shown that point clouds compare well with the voxel-based representation, such as performance and accuracy. Our work opens up multiple roads for future research. The proposed framework learns to predict shape, texture, and pose from single images, without rendering step, based solely on 2D projections of 3D point clouds and their coverage of the ground-truth silhouette. While rendering requires exhaustive computation, our key finding is that it does not endow accuracy in 3D structure learning. Our system achieves state-of-the-art results by simultaneously minimising modified first term loss and second term loss based on the invariance of the structure. We evaluate our approach on ShapeNet (for generated 3D point clouds) and on CUB-200-2011 and Pascal3D+ (for the final 3D output) datasets and demonstrate its high adaptivity and performance level. Also, we show and discuss the efficiency and robustness of our model.

References

- [1] Eman Ahmed, Alexandre Saint, Abd El Rahman Shabayek, Kseniya Cherenkova, Rig Das, Gleb Gusev, Djamila Aouada, and Bjorn Ottersten. A survey on deep learning advances on different 3d data representations, 2019.
- [2] Angel X. Chang, Thomas Funkhouser, Leonidas Guibas, Pat Hanrahan, Qixing Huang, Zimo Li, Silvio Savarese, Manolis Savva, Shuran Song, Hao Su, Jianxiong Xiao, Li Yi, and Fisher Yu. Shapenet: An information-rich 3d model repository, 2015.
- [3] Wenzheng Chen, Huan Ling, Jun Gao, Edward Smith, Jaakko Lehtinen, Alec Jacobson, and Sanja Fidler. Learning to predict 3d objects with an interpolation-based differentiable renderer. In H. Wallach, H. Larochelle, A. Beygelzimer, F. d'Alché-Buc, E. Fox, and R. Garnett, editors, *Advances in Neural Information Processing Systems*, volume 32, pages 9609–9619. Curran Associates, Inc., 2019.
- [4] Mehdi Chouchane, Alexis Rucci, and Alejandro A Franco. A versatile and efficient voxelization-based meshing algorithm of multiple phases. *ACS omega*, 4(6):11141–11144, 2019.
- [5] Christopher B. Choy, Danfei Xu, JunYoung Gwak, Kevin Chen, and Silvio Savarese. 3d-r2n2: A unified approach for single and multi-view 3d object reconstruction, 2016.
- [6] Blender Online Community. *Blender - a 3D modelling and rendering package*. Blender Foundation, Stichting Blender Foundation, Amsterdam, 2018.
- [7] Thibault Groueix, Matthew Fisher, Vladimir G. Kim, Bryan C. Russell, and Mathieu Aubry. Atlasnet: A papier-mâché approach to learning 3d surface generation, 2018.
- [8] Z. Han, Z. Liu, J. Han, C. Vong, S. Bu, and X. Li. Unsupervised 3d local feature learning by circle convolutional restricted boltzmann machine. *IEEE Transactions on Image Processing*, 25(11):5331–5344, 2016.
- [9] Martin Heusel, Hubert Ramsauer, Thomas Unterthiner, Bernhard Nessler, and Sepp Hochreiter. Gans trained by a two time-scale update rule converge to a local nash equilibrium, 2018.
- [10] Eldar Insafutdinov and Alexey Dosovitskiy. Unsupervised learning of shape and pose with differentiable point clouds. *CoRR*, abs/1810.09381, 2018.
- [11] Danilo Jimenez Rezende, S. M. Ali Eslami, Shakir Mohamed, Peter Battaglia, Max Jaderberg, and Nicolas Heess. Unsupervised learning of 3d structure from images. In D. Lee, M. Sugiyama, U. Luxburg, I. Guyon, and R. Garnett, editors, *Advances in Neural Information Processing Systems*, volume 29, pages 4996–5004. Curran Associates, Inc., 2016.
- [12] Angjoo Kanazawa, Shubham Tulsiani, Alexei A. Efros, and Jitendra Malik. Learning category-specific mesh reconstruction from image collections, 2018.
- [13] Hiroharu Kato, Deniz Beker, Mihai Morariu, Takahiro Ando, Toru Matsuoka, Wadim Kehl, and Adrien Gaidon. Differentiable rendering: A survey, 2020.
- [14] Michael Kazhdan, Matthew Bolitho, and Hugues Hoppe. Poisson surface reconstruction. In *Proceedings of the Fourth Eurographics Symposium on Geometry Processing*, SGP '06, page 61–70, Goslar, DEU, 2006. Eurographics Association.
- [15] Tarun Kumar and Karun Verma. A theory based on conversion of rgb image to gray image. *International Journal of Computer Applications*, 7(2):7–10, 2010.

- [16] Yuanzhuo Li, Yunan Zheng, Jie Chen, Zhenyu Xu, and Yiguang Liu. Learning structural coherence via generative adversarial network for single image super-resolution, 2021.
- [17] Zhengqin Li, Mohammad Shafiei, Ravi Ramamoorthi, Kalyan Sunkavalli, and Manmohan Chandraker. Inverse rendering for complex indoor scenes: Shape, spatially-varying lighting and svbrdf from a single image, 2019.
- [18] Jinxue Liu and Hancheng Lu. Imnet: A learning based detector for index modulation aided mimo-ofdm systems, 2019.
- [19] Sainan Liu, Vincent Nguyen, Isaac Rehg, and Zhuowen Tu. Recognizing objects from any view with object and viewer-centered representations. In *Proceedings of the IEEE/CVF Conference on Computer Vision and Pattern Recognition (CVPR)*, June 2020.
- [20] Shaohui Liu, Yinda Zhang, Songyou Peng, Boxin Shi, Marc Pollefeys, and Zhaopeng Cui. Dist: Rendering deep implicit signed distance function with differentiable sphere tracing, 2020.
- [21] Shichen Liu, Weikai Chen, Tianye Li, and Hao Li. Soft rasterizer: Differentiable rendering for unsupervised single-view mesh reconstruction, 2019.
- [22] Matthew M Loper and Michael J Black. Opendr: An approximate differentiable renderer. In *European Conference on Computer Vision*, pages 154–169. Springer, 2014.
- [23] Lars Mescheder, Michael Oechsle, Michael Niemeyer, Sebastian Nowozin, and Andreas Geiger. Occupancy networks: Learning 3d reconstruction in function space, 2019.
- [24] E. Mouragnon, M. Lhuillier, M. Dhome, F. Dekeyser, and P. Sayd. Real time localization and 3d reconstruction. In *2006 IEEE Computer Society Conference on Computer Vision and Pattern Recognition (CVPR'06)*, volume 1, pages 363–370, 2006.
- [25] Thu Nguyen-Phuoc, Chuan Li, Stephen Balaban, and Yong-Liang Yang. Rendernet: A deep convolutional network for differentiable rendering from 3d shapes, 2019.
- [26] Michael Niemeyer, Lars Mescheder, Michael Oechsle, and Andreas Geiger. Differentiable volumetric rendering: Learning implicit 3d representations without 3d supervision, 2020.
- [27] G.S. Sreegadha. Image interpolation based on multi scale gradients. *Procedia Computer Science*, 85:713–724, 2016. International Conference on Computational Modelling and Security (CMS 2016).
- [28] Xingyuan Sun, Jiajun Wu, Xiuming Zhang, Zhoutong Zhang, Chengkai Zhang, Tianfan Xue, Joshua B. Tenenbaum, and William T. Freeman. Pix3d: Dataset and methods for single-image 3d shape modeling, 2018.
- [29] Maxim Tatarchenko, Alexey Dosovitskiy, and Thomas Brox. Octree generating networks: Efficient convolutional architectures for high-resolution 3d outputs, 2017.
- [30] Shubham Tulsiani, Alexei A. Efros, and Jitendra Malik. Multi-view consistency as supervisory signal for learning shape and pose prediction, 2018.
- [31] Shubham Tulsiani, Tinghui Zhou, Alexei A. Efros, and Jitendra Malik. Multi-view supervision for single-view reconstruction via differentiable ray consistency, 2017.
- [32] C. Wah, S. Branson, P. Welinder, P. Perona, and Serge J. Belongie. The caltech-ucsd birds-200-2011 dataset. 2011.
- [33] Nanyang Wang, Yinda Zhang, Zhuwen Li, Yanwei Fu, Wei Liu, and Yu-Gang Jiang. Pixel2mesh: Generating 3d mesh models from single rgb images, 2018.
- [34] Weiyue Wang, Duygu Ceylan, Radomir Mech, and Ulrich Neumann. 3dn: 3d deformation network, 2019.
- [35] Jiajun Wu, Yifan Wang, Tianfan Xue, Xingyuan Sun, William T Freeman, and Joshua B Tenenbaum. Marrnet: 3d shape reconstruction via 2.5d sketches, 2017.
- [36] Wenqi Xian, Patsorn Sangkloy, Varun Agrawal, Amit Raj, Jingwan Lu, Chen Fang, Fisher Yu, and James Hays. Texturegan: Controlling deep image synthesis with texture patches, 2018.
- [37] Yu Xiang, Roozbeh Mottaghi, and Silvio Savarese. Beyond pascal: A benchmark for 3d object detection in the wild. In *IEEE Winter Conference on Applications of Computer Vision (WACV)*, 2014.
- [38] Qiangeng Xu, Weiyue Wang, Duygu Ceylan, Radomir Mech, and Ulrich Neumann. Disn: Deep implicit surface network for high-quality single-view 3d reconstruction, 2019.
- [39] Richard Zhang, Phillip Isola, Alexei A. Efros, Eli Shechtman, and Oliver Wang. The unreasonable effectiveness of deep features as a perceptual metric, 2018.